frame value, as expected.[9] The results of a series of runs using different values of modulation index are also shown in Fig. 1(b). The agreement between theory and experiment is clear.

Other preliminary results have been obtained: (1) The experiment works efficiently in polycrystalline solids—we have succeeded in reducing the linewidth of the proton spectrum in adamantane by two orders of magnitude. Since the linewidth at this point is the same as that of a liquid sample, rf-field inhomogeneity appears to be the limiting factor. (2) Reduction of the dipolar coupling is just as dramatic when the rf is off resonance, and we have observed preservation of chemical-shift structure in liquids under these conditions. Thus, the potential exists for uncovering chemical-shift anisotropies and heteronuclear couplings obscured by homonuclear broadening. (3) The experiment works as well with frequency modulation of the rf field, and also for $\omega_M < \omega_1$. (4) A variety of multiple-quantum transitions are observed when modulation is used. (5) No reduction of the dipolar coupling is achieved when the requirements for photon dressing (i.e. $\omega_M \gg \omega_1$) are met.

These and other aspects of the experiment are under investigation and will be reported on in more complete form.

We thank R. D. Kendrick for technical assistance, F. F. Abraham for help with DSL/360, and D. E. Horne for help with the spectrometer.

*Present address: Max-Planck-Institut für Medikalische Forschung, Abteilung für Moleculare Physik, Jahnstrasse 29, 6900 Heidelberg, W. Germany.

[1]C. Cohen-Tannoudji and S. Haroche, C. R. Acad. Sci. 262, 268 (1966); M. Kunitomo and T. Hashi, Phys. Lett. 40A, 75 (1972).

[2]A. G. Redfield, Phys. Rev. 98, 1787 (1955).

[3]DSL/360 is an IBM program for the digital simulation of continuous-system dynamics.

[4]F. Bloch and A. Siegert, Phys. Rev. 57, 522 (1940).

[5]F. Ansbacher, J. Phys. B 6, 1620, 1633 (1973).

[6]C. S. Yannoni, J. Am. Chem. Soc. 91, 4611 (1969).

[7]H. C. Torrey, Phys. Rev. 76, 1059 (1949).

[8]E. P. Jones and S. R. Hartmann, Phys. Rev. B 6, 757 (1972).

[9]D. Barnaal and I. J. Lowe, Phys. Rev. Lett. 11, 258 (1963).

Electronic Momentum Densities by Two-Dimensional Angular Correlation of Annihilation Radiation in Aluminum*

J. Mader, S. Berko, H. Krakauer,† and A. Bansil‡
Department of Physics, Brandeis University, Waltham, Massachusetts 02154
(Received 2 July 1976)

Two-dimensional angular correlation of two γ's from positrons annihilating in aluminum have been measured with a multidetector apparatus and compared with momentum densities based on orthogonal-plane-wave electron wave functions. Anisotropy in the momentum distributions and direct evidence for annihilation with the high-momentum components of the conduction band are found.

In this Letter we report the first two-dimensional (2D) angular correlation measurements of 2γ annihilation radiation from oriented single crystals of aluminum, and compare the results with theoretical predictions. The experiments were performed to test the sensitivity of the technique to the electron and positron wave functions and, in particular, to study the nature of the high-momentum components (HMC) of the correlations in a simple metal.

The applicability of the positron technique to the study of electronic band structure[1] and particularly of Fermi surfaces[2] (FS) is well known. In the independent-particle model (IPM) the momentum distribution $\rho(\vec{p})$ carried by the annihilation photons from a periodic lattice at zero temperature is given by[1]

$$\rho(\vec{p}) = \text{const} \sum_{\vec{k},n} \left| \int d^3r \exp(-i\vec{p}\cdot\vec{r}) u_0^+(\vec{r}) u_{\vec{k},n}^-(\vec{r}) \exp(i\vec{k}\cdot\vec{r}) \right|^2 = \text{const} \sum_{\vec{k},n} \sum_{\vec{G}} A_{\vec{G}}(\vec{k}, n) |^2 \delta(\vec{p}-\vec{k}-\vec{G}), \quad (1)$$

where $u_0^+(\vec{r})$ is the ground-state ($\vec{k}=0$) positron Bloch wave function $u_{\vec{k},n}^-(\vec{r}) \exp(i\vec{k}\cdot\vec{r})$ is the electron wave function with crystal momentum $\vec{k}$ and band index n, $\vec{G}$ is a reciprocal lattice vector, and

$$u_0^+(\vec{r}) u_{\vec{k},n}^-(\vec{r}) = \sum_{\vec{G}} A_{\vec{G}}(\vec{k}, n) \exp(i\vec{G}\cdot\vec{r});$$

$\hbar \equiv 1$. The summation is over all occupied states in the first zone.

As discussed by Berko and Plaskett,[3] one obtains from Eq. (1) a distribution $\rho(\vec{p})$ exhibiting breaks not only at the FS in the first zone ($\vec{p} = \vec{k}$), but also in higher zones, due to the HMC of the e^- and e^+ wave functions ("umklapp annihilations"). One therefore predicts a set of Fermi surfaces in $\vec{p}$ space modulated at each $\vec{p} = \vec{k} + \vec{G}$ by $|A_{\vec{G}}(\vec{k}, n)|^2$. Thus the measurement of $\rho(\vec{p})$ by angular correlations reflects the shape and size of the FS, as well as the nature of the wave functions via the Fourier coefficients $A_{\vec{G}}(\vec{k}, n)$. Additionally, deviations are expected from the IPM predictions due to many-body correlations[1]; these deviations can be expressed as a momentum-dependent enhancement factor[4] $E(\vec{p})$ multiplying the IPM $\rho(\vec{p})$.

In angular correlation measurements one usually uses "long-slit" geometry to obtain $N(p_z) = \int\int \rho(\vec{p}) dp_x dp_y$, where $p_z = \theta mc$, θ being the angle measured. More rarely, "crossed-slit" 2D curves $N(p_z, p_y) = \int \rho(\vec{p}) dp_x$ are obtained in measurements usually confined to internal e^+ sources of Cu or Cu-based alloys.[2] In this Letter we present detailed "crossed-slit" measurements employing an external positron source; the intrinsic low counting rate of the 2D geometry has been compensated for by using multiple pairs of counters. We selected aluminum as a test metal because its nearly free-electronlike band structure is well known[5] and because in long-slit measurements it exhibits a well-defined but low-intensity high-momentum tail.[3] Usually these tails are attributed to annihilation with core electrons. However, HMC of the conduction band have been inferred from anisotropy studies of long-slit data in Cu[6] and in Ge.[7] The crossed-slit geometry permits a direct observation of these conduction-band HMC.

The 2D measurements were performed with a multicounter correlation apparatus[8] using 22 5-cm-long by 3.8-cm-diam NaI detectors behind Pb collimating slits subtending 0.5×2.2 mrad at the sample; the sample-to-counter distance is 320 cm. The aluminum single crystals were 1.5-mm-thick, 10-mm-diam disks, annealed for 24 h at 610°C and slowly cooled; in the experiment they were kept at 100°K on a cold finger. The positrons from an external Co^{58} source (up to 500 mCi) were focused onto the sample face by a 17-kG magnetic field. The experiments were performed with p_y fixed, scanning along the p_z direction. The orientations are indicated by the notation Al$[p_z], [p_x]$. In Fig. 1 we present the meas-

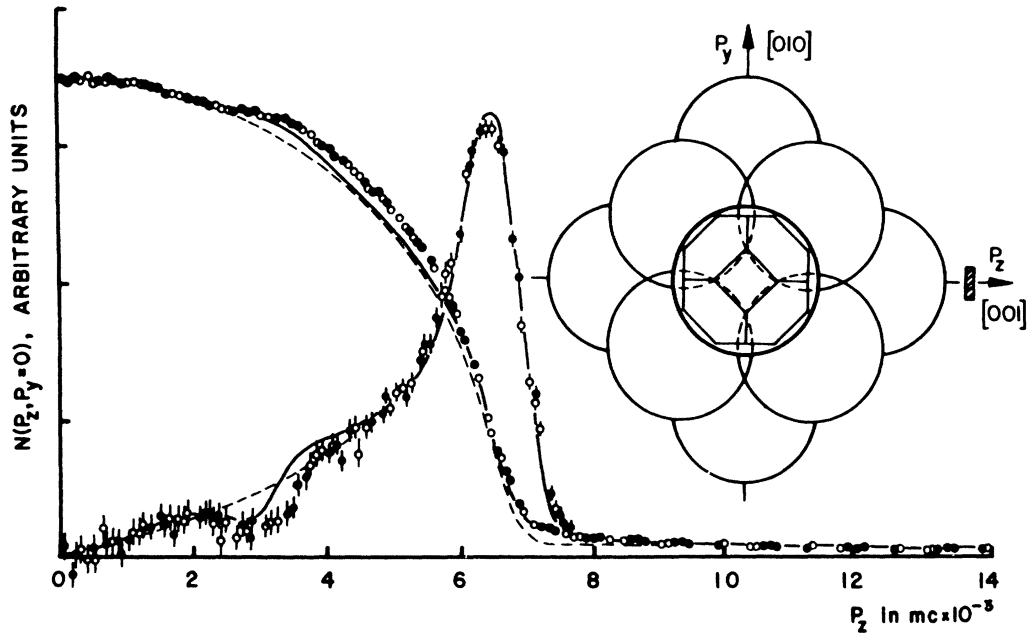

FIG. 1. Al[001], [100] angular correlation with $p_y = 0$, and the absolute magnitude of the first derivative (second nearest neighbors). One unit of $mc \times 10^{-3}$ corresponds to an angle of 1 mrad. Open circles correspond to $p_z < 0$ folded about $p_z = 0$ to exhibit the inherent symmetry of the data. Full curve is the theoretical OPW prediction; dashed curve corresponds to simple sphere model discussed in text. The inset indicates the projection of the BZ and of the (111) and (200) spheres used in the simple model onto the (100) plane. The shaded rectangle indicates the effective resolution along p_z and p_y; integration direction is perpendicular to the plane of the inset.

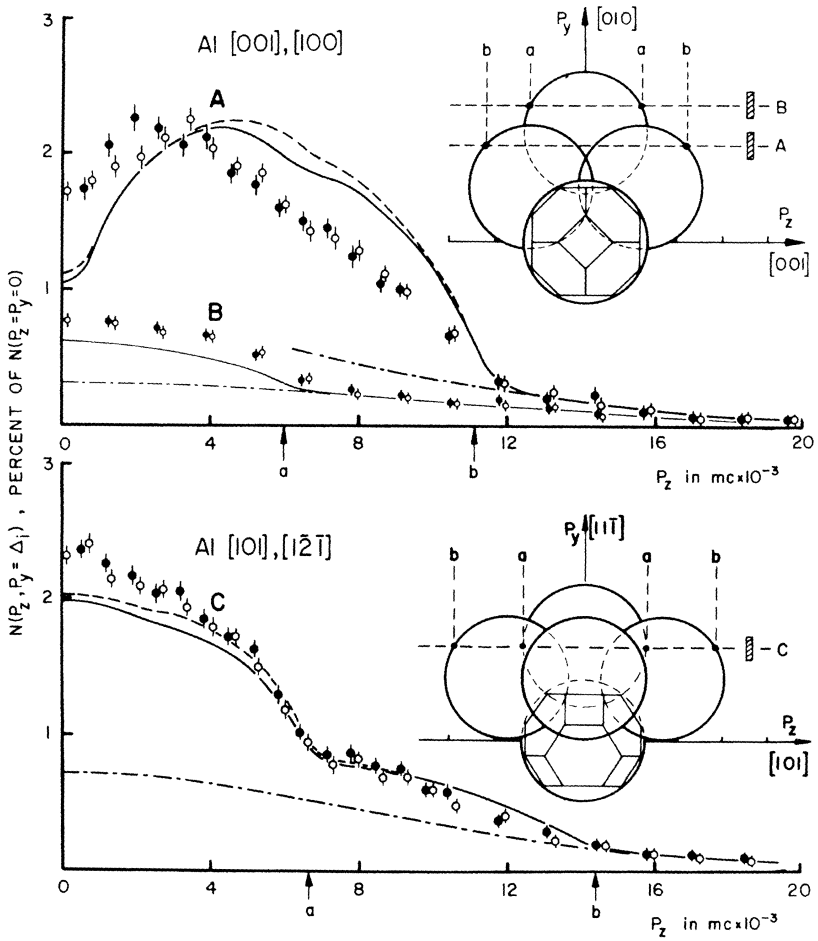

FIG. 2. High-momentum measurements at constant $p_y = \Delta_i = |G_{111}| = 10.41 \times 10^{-3} mc$ for Al[001],[100] (curve A) and Al[101], [1$\bar{2}\bar{1}$] (curve C), and $\Delta_i = 15 \times 10^{-3} mc$ for Al[001],[100] (curve B). The dash-dotted line corresponds to the continuation of the IPM core contribution plotted with half intensity as discussed in text. The theoretical curves and the inset are as in Fig. 1.

urement of $N(p_z, p_y)$ at $p_y = 0$ for the Al[001], [100] orientation and in Fig. 2 we plot three representative curves obtained at finite p_y to study nature of the HMC.

The experimental curves are compared with theoretical momentum densities.[9] The conduction-band wave functions were computed as a linear combination of four orthogonal plane waves (OPW's),[10] using the Fourier coefficients V_{111} and V_{200} and the effective mass found by Segall[5] to reproduce best his Korringa-Kohn-Rostoker bands. Tight-binding core states were constructed from Herman and Skillman free-atom orbitals and the explicit orthogonalization terms were included for the valence functions. The positron wave function was calculated as an expansion in symmetrized plane waves using an inverted lattice potential.[11] The full $\rho(\vec{p})$ was computed by adding to the valence $\rho(\vec{p})$ one half of the IPM core $\rho(\vec{p})$. The reason for this lowering of the theoretical core amplitude will be discussed in connection with Fig. 2. The theoretical momentum profiles $\rho(\vec{p})$ along various $\vec{p}$ directions indicate that, except at momenta close to the zone faces where the deviations from free-electron behavior follow closely the nearly free electron predictions, the momentum density is nearly $\vec{k}$ independent. Thus, following Ref. 3, a much simplified model was also used. In this "Wigner-Seitz" model a free-electron sphere was centered on each reciprocal lattice site $\vec{G}$, and weighted uniformly by $|A_{\vec{G}}(0)|^2$ taken from the full IPM theory described above.[12] In order to compare theory with experiment the theoretical $\rho(\vec{p})$'s were integrated along one of the components (p_x) and the experimental momentum resolutions along p_y and p_z were folded in; the theoretical curves $N(p_z, p_y)$ were normalized to the experimental value at $p_z = p_y = 0$.

In Fig. 1 we plot the Al[001], [100] curve, with $p_y = 0$. In order to exhibit the fine structure in the curve, the derivative of the data is also plotted.[2] We scaled $N(p_z, p_y = 0)$ in such a way as to demonstrate the nearly circular nature of the central curve, as expected for a free-electron gas with perfect momentum resolution. The experimental curve exhibits an extended bulge compared to the IPM computations, which, as known from long-slit experiments on alkali metals, is attributable to e^+-e^- many-body effects.[1,4,10] Indeed, good agreement can be obtained between the "model curve" (dashed line) and experiment after the theoretical many-body isotropic enhancement $E(p)$ of the interacting positron-electron gas[4] is included in the model computation. On the other hand, the simple model clearly fails to reproduce the structure in the distribution observed around $p_z = 3 \times 10^{-3} mc$. This structure, particularly clear in the derivative curve, is well reproduced by the OPW computation (full curve), and is thus attributable to zone face interactions. This effect is due to points close to the Brillouin-zone (BZ) corner W, where the FS is closest to the zone boundary and thus the wave functions deviate most from free behavior. More precise experiments and more detailed calculations will be required to separate the effects of FS topology from the $\vec{k}$ dependence of the $|A_{\vec{G}}(\vec{k})|^2$ in this region. Deviations from free-electron behavior can also be clearly observed just outside the first Fermi surface, around $p_z = 7 \times 10^{-3} mc$, where the OPW curve clearly fits the experiment better than does the simple model.

Other distribution curves with $p_y = 0$ were obtained with the following orientations: [001], [110]; [101], [10$\bar{1}$]; [101], [10$\bar{1}$]; [101], [1$\bar{2}\bar{1}$]; [111], [11$\bar{2}$]. These curves indicate that the many-body "bulge" is isotropic. The fine structure is anisotropic and again appears to be correlated with the position of the W point. The difference curves ("anisotropies") show a complex structure of up to 2.5% amplitude and are reasonably reproduced by the OPW theory.

Although these particular experiments were not performed to measure the values of the FS radii accurately, we have ascertained p_F by analyzing the break at the FS as smeared by the angular resolution. We obtain $p_F[100] = (6.73 \pm 0.03) \times 10^{-3} mc$, $p_F(111) = (6.79 \pm 0.04) \times 10^{-3} mc$, and $p_F[110] = (6.67 \pm 0.08) \times 10^{-3} mc$, compared to the free-electron value of $6.78 \times 10^{-3} mc$ at 100°K. We note that improved statistics and resolution in the FS region can yield, in principle, higher precision measurements for these values; the crossed-slit geometry is superior to the long-slit geometry because, for the same p_z resolution, the slope at the break is sharper, and less HMC enter the integrated region.

Note that in Fig. 1 the tail of the distribution is but a few percent of the distribution at $p_z = 0$, $p_y = 0$. Figure 2 shows the ability of the 2D system to detect structure within this tail, by setting p_y large enough to avoid the main FS and scanning along p_z (see insets). The curves of Fig. 2 are plotted as percentages of $N(p_z, p_y)$ at $p_z = p_y = 0$. An inspection of the three measurements presented in Fig. 2 with regard to the geometry of the umklapp Fermi spheres shown in the insets clearly indicates that much of the tail distribution is due to umklapp annihilations. One can easily identify the breaks at the FS of the umklapp spheres with breaks in the angular distributions marked *a* and *b*. Outside of the (111) and (200) spheres the umklapp contribution is predicted to be negligible and one expects mainly annihilation with core electrons. It is when fitting this region of momentum space that we are forced to lower the IPM core intensity by a factor of 2. The good fit of the core shape with one-half intensity is particularly evident in curve *B* ($p_y = 15 \times 10^{-3} mc$) for $p_z > 7 \times 10^{-3} mc$.

To analyze the sensitivity of the umklapp curves to the theoretical IPM parameters, we have recomputed IPM conduction-band distributions without the core orthogonalizing terms. These curves were superimposed on half the IPM core distribution as discussed above. We find that leaving the orthogonalization terms out substantially underestimates the HMC (by approximately a factor of 2). Thus the 2D distributions are sensitive enough to distinguish between the OPW and the pseudo wave function.

We find that using an alternative realistic positron wave function[11] in Al changes the core intensity by at most 15%; in addition, the core momentum density obtained with ψ^+ set constant reproduces well the density based on Hartree-Fock core wave functions. It is therefore reasonable to assume that the required reduction by a factor of 2 is due to a $\vec{k}$-independent, many-body core enhancement term, as predicted theoretically by Carbotte and Salvadori.[13] The reduction of the IPM intensity by 2 corresponds to a core-enhancement (E_{core}) factor of 2 lower than the overall enhancement for conduction electrons (E_{cond}). The theoretical ratio of the enhancement factors[13] for Al was found to be $E_{cond}/E_{core} = 1.5$, reasonab-

ly close to our observed value of 2. Similar behavior was inferred some time ago by Terrell, Weisberg, and Berko[14] in alkali metals, by comparing the theoretical and experimental angular distributions with the corresponding annihilation rates; they find a ratio $E_{cond}/E_{core}=4$.

Returning to the conduction-band umklapp annihilations of Fig. 2, the theoretical curves (OPW as well as sphere model) fit the experimental curves for the [101], [1$\bar{2}\bar{1}$] orientation well, but deviate somewhat for the [001], [100] orientation in shape, but not in amplitude. More detailed work will have to be performed to understand the origin of these deviations. From our ability to use the IPM amplitude for the umklapp curves we conclude that the many-body enhancement does not change these amplitudes appreciably, as predicted theoretically by Hede and Carbotte.[15]

We would like to thank L. Schwartz for helpful discussions and for critical reading of this manuscript.

*Work supported by the National Science Foundation.

†Present address: Department of Physics, West Virginia University, Morgantown, W. V. 26506.

‡Present address: Department of Physics, Northeastern University, Boston, Mass. 02215.

[1]For a recent review, see R. N. West, Adv. Phys. 22, 263 (1973).

[2]S. Berko and J. Mader, Appl. Phys. 5, 287 (1975).

[3]S. Berko and J. S. Plaskett, Phys. Rev. 112, 1877 (1958).

[4]J. P. Carbotte and S. Kahana, Phys. Rev. 139, A213 (1965), and references quoted therein.

[5]B. Segall, Phys. Rev. 124, 1797 (1961).

[6]S. Cushner, J. C. Erskine, and S. Berko, Phys. Rev. B 1, 2852 (1970).

[7]M. A. Shulman, G. M. Beardsley, and S. Berko, Appl. Phys. 5, 367 (1975).

[8]For details see J. Mader, Ph.D. thesis, Brandeis University, 1975 (unpublished); the anisotropic enhancement suggested from the data in the thesis was later found to be due to a side effect of the spark-cutting process which vanished after proper annealing—probably e^+ trapping in imperfections from surface damage not detected by standard Laue pictures.

[9]For more details regarding the theoretical computations see H. Krakauer, Ph.D. thesis, Brandeis University, 1975 (unpublished).

[10]The secular equation used to construct the conduction wave functions was taken from the work of W. A. Harrison, Phys. Rev. 118, (1960), as in the work of D. Stroud and H. Ehrenreich, Phys. Rev. 171, 399 (1968). The latter authors, however, did not include the effects of core orthangonalization.

[11]A truncated expansion in symmetrized plane waves using 145 terms was obtained which compared reasonably well with the e^+ wave function obtained by a pseudopotential approach by P. Kubica and M. J. Stott, J. Phys. F 4, 1969 (1974). In using the negative of the electronic potential, we are ignoring the fact that the positron is not subject to any exchange effects. A comparison of our results with those obtained using the positron wave function of Stroud and Ehrenreich (Ref. 10) indicates that these effects lead to errors in $\rho(\vec{p})$ of less than 2% for $p \leq p_F$ and no greater than 15% for $p \geq p_F$.

[12]The values used were $|A_{(000)}(0)|^2=0.957$, $|A_{(111)}(0)|^2=0.0097$, and $|A_{(200)}(0)|^2=0.0030$.

[13]J. P. Carbotte and A. Salvadori, Phys. Rev. 162, 290 (1967).

[14]J. H. Terrell, H. L. Weisberg, and S. Berko, *Positron Annihilation* (Academic, New York, 1967), p. 269.

[15]B. B. J. Hede and J. P. Carbotte, J. Phys. Chem. Solids 33, 727 (1972).

Dependence of the Ion Current on Voltage in a Reflex Triode

C. A. Kapetanakos, J. Golden, and W. M. Black*
Naval Research Laboratory, Washington, D. C. 20375
(Received 12 August 1976)

Results are reported on the dependence of the current of a pulsed ion beam produced in a reflex triode upon the applied resistive voltage in the range 0.6 to 1.3 MV. The measured peak ion current at the maximum voltage tested is 20 kA, corresponding to a current density of 200 A/cm^3.

During the last few years, there has been increased interest on the production of intense ion beams[1-11] with use of the existing pulsed power technology initially developed for the generation of relativistic electron pulses. Recent intensive studies of such ion beams have furnished valuable information on their properties and propagation characteristics. However, presently very little is known about the scaling of their current with the applied voltage. In this Letter, we report experimental results on the variation of the ion current (I_i) with applied resistive voltage (V_0) in the range 0.6 to 1.3 MV.

A schematic diagram of the experiment is